

Current-induced Spin Polarization in Two-Dimensional Hole Gas

Chao-Xing Liu^{1,2}, Bin Zhou², Shun-Qing Shen², and Bang-fen Zhu¹

¹*Department of Physics and Center for Advanced Study, Tsinghua University, Beijing 100084, China*

²*Department of Physics and Center of Computational and Theoretical Physics,
The University of Hong Kong, Hong Kong, China*

(Dated: November 20, 2018)

We investigate the current-induced spin polarization in the two-dimensional hole gas (2DHG) with the structure inversion asymmetry. By using the perturbation theory, we re-derive the effective k -cubic Rashba Hamiltonian for 2DHG and the generalized spin operators accordingly. Then based on the linear response theory we calculate the current-induced spin polarization both analytically and numerically with the disorder effect considered. We have found that, quite different from the two-dimensional electron gas, the spin polarization in 2DHG depends linearly on Fermi energy in the low doping regime, and with increasing Fermi energy, the spin polarization may be suppressed and even changes its sign. We predict a pronounced peak of the spin polarization in 2DHG once the Fermi level is somewhere between minimum points of two spin-split branches of the lowest light-hole subband. We discuss the possibility of measurements in experiments as regards the temperature and the width of quantum wells.

PACS numbers: 72.25.-b, 85.75.-d, 71.70.Ej, 72.25.Pn

I. INTRODUCTION

In order to reduce the electric leakage and to meet the challenge brought about by the reduced physical size of the future nano-electronics, it is being explored to replace the electron charge with the spin degree of freedom in the electronic transport. This is the ambitious goal of researchers in the field of spintronics.^{1,2,3} One of basic issues in this field is how to generate the polarized spin in devices. As a straightforward way, the spin injection from ferromagnetic layers may provide a possible solution to this problem if the interface mismatch problem can be avoided, but it is more desirable to generate spin polarization directly by electric means in devices because of its easy controllability and compatibility with the standard microelectronics technology.^{1,2,3} The spin-orbit coupling (SOC) in semiconductors, which relates the electron spin to its momentum, may provide a controllable way to realize such purpose. Based on this idea, the phenomenon of current-induced spin polarization (CISP) has recently attracted extensive attentions of a lot of research groups.^{4,5,6,7,8,9,10,11,12,13,14,15,16,17,18,19,20,21,22,23,24,25,26}

As early as in 1970's, the CISP due to the spin-orbit scattering near the surface of semiconductor thin films was predicted by Dyakonov and Perel.⁴ Restricted by experimental conditions at that time, this prediction was ignored until the beginning of 1990's. With the development of sample fabrication and characterization technology in low-dimensional semiconductor systems, it was realized that such phenomena could also exist in quantum wells and heterostructures with the structure or bulk inversion asymmetry.^{5,6} Later, many interesting topics about CISP have been raised, such as the joint effect of the Rashba and Dresselhaus SOC mechanism,⁷ vertex correction,^{5,6,7,8} quantum correction^{9,10} and resonant spin polarization.¹¹ Experimentally, CISP was first observed by Silov *et al*¹² in two-dimensional

hole gas (2DHG) by using the polarized photoluminescence.^{27,28,29} When inputting an in-plane current into the 2DHG system, they observed a large optical polarization in photoluminescence spectra.¹² Later, Kato *et al* demonstrated the existence of the CISP in strained nonmagnetic semiconductors,^{13,14} and Sih *et al* detected the CISP in the two-dimensional electron gas (2DEG) in (110) *AlGaAs* quantum well.¹⁵ The CISP was also found in *ZnSe* epilayers even up to the room temperature.¹⁶ Very recently, the converse effect of CISP has been clearly shown by Yang *et al* experimentally,¹⁷ and the spin photocurrent has also been observed.^{18,19,20}

So far most theoretic investigations about the CISP deal with the electron SOC systems.^{4,5,6,7,8,9,10,21,22,23,24,25,26} Thus the CISP in the 2DHG system as shown in Silov's experiments was also interpreted in terms of the linear- k Rashba coupling of the 2DEG systems with several parameters adjusted.¹² As we shall show later, this treatment is not appropriate for 2DHG. Unlike the electron system, the hole state in the Luttinger-Kohn Hamiltonian³⁰ is a spinor of four components. As each component is a combination of spin and orbit momentum, the spin of a hole spinor is not a conserved physical quantity. Therefore, the "spintronics" for hole gas is in fact a combination of spintronics and orbitronics³¹. If only the lowest heavy hole (HH1) subband is concerned, by projecting the multi-band Hamiltonian of 2DHG with structural inversion asymmetry into a subspace spanned by $|\pm \frac{3}{2}\rangle$ mostly relevant with the HH1 states, we can obtain the k -cubic Rashba model^{32,33,34,35,36}. We emphasize here in this lowest heavy hole subspace, the spin operators are no longer represented by three Pauli matrices, because the "generalized spin" we shall adopt is a hybridization of spin and orbit angular momentum. In deriving the effective Hamiltonian from the Luttinger-Kohn Hamiltonian by the perturbation and truncation

procedure to higher orders, one must take care of the corresponding transformation for the spin operator in order to obtain the correct expression. In the following, we will use the terminology "generalized spin", or the "spin" for short, to denote the total angular momentum in the spin-orbit coupled systems.

The aim of the present paper is to investigate the CISP of 2DHG in a more rigorous way. Namely, we will derive the k -cubic Rashba model and the corresponding spin operators for holes, and on this basis we will present both analytical and numerical results for the CISP in 2DHG. This paper is organized as follows. In Sec II the general formalism and the Hamiltonian for the 2DHG with structural inversion asymmetry is given. In Sec III in the low doping regime, with the perturbation theory, the Hamiltonian and spin operators in the lowest heavy hole subspace are derived, and applied to analytical calculation of the CISP in 2DHG. In Sec IV, we will show the numerical calculations agree well with the analytical results at the low-doping regime; while in the high doping regime the numerical results predict some new features of CISP. Particularly, we predict a pronounced CISP peak when Fermi energy lies little above the energy minimum of the lowest light hole (LH1) subband. Finally, a brief summary is drawn.

II. FORMALISM

A. Hole Hamiltonian

A p-doped quantum well system with structural inversion asymmetry can be described as the isotropic Luttinger-Kohn Hamiltonian with a confining asymmetrical potential,

$$\hat{H} = \hat{H}_L + \hat{V}_c(z) + \hat{V}_a(z). \quad (1)$$

Here in order to compare the analytical results with the numerical one, the confining potential along the z -direction $V_c(z)$ is taken as

$$\hat{V}_c(z) = \begin{cases} 0 & -L_z/2 < z < L_z/2 \\ \infty & \text{otherwise,} \end{cases} \quad (2)$$

where L_z is the well width of the quantum well. The asymmetrical potential, which stems from a build-in electric field F via the gate voltage or δ -doping is $\hat{V}_a(z) = eFz$, which breaks the inversion symmetry and lifts the spin doublet degeneracy.

Let \hat{S} be the generalized spin operator of a hole state, and \hat{S}_z be the z -component of \hat{S} , the isotropic Luttinger-Kohn Hamiltonian \hat{H}_L in the $|S, S_z\rangle$ representation (four basis kets written in the sequence of $\{|\frac{3}{2}\rangle, |\frac{1}{2}\rangle, |-\frac{1}{2}\rangle, |-\frac{3}{2}\rangle\}$) is expressed as

$$\hat{H}_L = \begin{pmatrix} P & R & T & 0 \\ R^\dagger & Q & 0 & T \\ T^\dagger & 0 & Q & -R \\ 0 & T^\dagger & -R^\dagger & P \end{pmatrix}, \quad (3)$$

with

$$P = \frac{\hbar^2}{2m_0}[(\gamma_1 + \gamma_2)\mathbf{k}^2 + (\gamma_1 - 2\gamma_2)k_z^2], \quad (4)$$

$$Q = \frac{\hbar^2}{2m_0}[(\gamma_1 - \gamma_2)\mathbf{k}^2 + (\gamma_1 + 2\gamma_2)k_z^2], \quad (5)$$

$$R = -\frac{\hbar^2\sqrt{3}\gamma_2}{m_0}\mathbf{k}_-k_z, \quad (6)$$

$$T = -\frac{\hbar^2\sqrt{3}\gamma_2}{2m_0}\mathbf{k}_-^2, \quad (7)$$

where γ_1, γ_2 is the Luttinger parameters, m_0 is the free electron mass, the in-plane wave vector $\mathbf{k} = (k_x, k_y)$, denoted in the polar coordinate as $\mathbf{k} \equiv (k, \theta)$, $\mathbf{k}_\pm \equiv k_x \pm ik_y$ and $k_z = -i\partial/\partial z$. The other terms, such as anisotropic term, C terms or hole Rashba term,^{35,36,37} have only negligible effects and are omitted in our calculation. Correspondingly, the x -, y -, z - component of the "spin"- $\frac{3}{2}$ operator respectively reads

$$\hat{S}_x = \frac{1}{2} \begin{pmatrix} 0 & \sqrt{3} & 0 & 0 \\ \sqrt{3} & 0 & 2 & 0 \\ 0 & 2 & 0 & \sqrt{3} \\ 0 & 0 & \sqrt{3} & 0 \end{pmatrix}, \quad (8)$$

$$\hat{S}_y = \frac{i}{2} \begin{pmatrix} 0 & -\sqrt{3} & 0 & 0 \\ \sqrt{3} & 0 & -2 & 0 \\ 0 & 2 & 0 & -\sqrt{3} \\ 0 & 0 & \sqrt{3} & 0 \end{pmatrix}, \quad (9)$$

$$\hat{S}_z = \frac{1}{2} \begin{pmatrix} 3 & 0 & 0 & 0 \\ 0 & 1 & 0 & 0 \\ 0 & 0 & -1 & 0 \\ 0 & 0 & 0 & -3 \end{pmatrix}. \quad (10)$$

We stress here again that the "spin" of the $\frac{3}{2}$ spinor is actually its total angular momentum, which is a linear combination of spin and orbit angular momentum of a valence band electron. In polarized optical experiments, such as polarized photoluminescence^{27,28,29} or Kerr/Farady rotation^{13,14}, it is appropriate to introduce such a generalized spin.

For the infinitely confining potential, we expand the eigenfunction ϕ_ν associated with the ν th hole subband in terms of confined standing waves as

$$\phi_\nu(\mathbf{k}) = \sum_{n, \lambda_h} a_{n, \lambda_h}^\nu(\mathbf{k}) \frac{1}{2\pi} e^{i\mathbf{k}\cdot\mathbf{r}} |n, \lambda_h\rangle_h, \quad (11)$$

with

$$|n, \lambda_h\rangle = \sqrt{\frac{2}{L_z}} \sin\left(\frac{n\pi(z + L_z/2)}{L_z}\right) |\lambda_h\rangle, \quad (12)$$

where $\mathbf{r} = (x, y)$, n is the confinement quantum number for the standing wave along the z -direction,

and λ_h denotes the λ_h -component of the hole ($\lambda_h = 3/2, 1/2, -1/2, -3/2$). Since we are only interested in the low energy physics, a finite number of n will result in a reasonable accuracy, and the effective Hamiltonian is reduced into a square matrix with a dimension of $4n$. In this way we obtain the hole subband structure analytically or numerically.

B. Expression for CISP

In the framework of the linear response theory, the electric response of spin polarization in a weak external electric field \mathbf{E} can be formulated as¹¹

$$\langle \hat{S}_\alpha \rangle = \sum_{\beta} \chi_{\alpha\beta} E_{\beta}, \quad (13)$$

where $\langle \hat{S}_\alpha \rangle$ is the thermodynamically averaged value of the spin density. The electric spin susceptibility $\chi_{\alpha\beta}$ can be calculated by Kubo formula.³⁸ By the Green function formalism, the Bastin version of Kubo formula³⁹ reads

$$\chi_{\alpha\beta} = \frac{ie\hbar}{2\pi} \int dE f(E) \text{Tr} \left\langle \hat{S}_\alpha \left(\frac{dG^R}{dE} v_\beta A - A v_\beta \frac{dG^A}{dE} \right) \right\rangle_c, \quad (14)$$

where G^R and G^A are the retarded and advanced Green function, respectively, $A = i(G^R - G^A)$ is the spectral function, $f(E)$ is the Fermi distribution function, v_β is the velocity operator along the β direction, and the bracket $\langle \dots \rangle_c$ represents the average over the impurity configuration.

To taken the vertex correction into account, we use the Streda-Smrcka division of Kubo formula,^{39,40}

$$\chi_{\alpha\beta} = -\frac{e\hbar}{2\pi} \int dE \frac{\partial f(E)}{\partial E} \text{Tr} \langle \hat{S}_\alpha G^R(E_F) v_\beta G^A(E_F) \rangle_c, \quad (15)$$

in which we retain only the non-analytical part, and neglect the analytical part, because the latter is much less important in the present case. In the following, we will use Eq. (15) to analytically calculate the electric spin susceptibility (ESS) with the vertex correction considered; meanwhile we will carry out the numerical calculation with Eq. (14) in the relaxation time approximation. We shall show that the analytical and numerical results are in good agreements with each other in the regime of low hole density.

C. Symmetry

The general properties of $\chi_{\alpha\beta}$ will be critically determined by symmetry of the system. For the two-dimensional system we investigate, the index $\alpha(\beta)$ in Eq. (13) is simply chosen to be x or y in the following. Without the asymmetrical potential V_a , the Hamiltonian

(1) is invariant under the space inversion transformation

$$\begin{aligned} x &\rightarrow -x, & y &\rightarrow -y, & z &\rightarrow -z, \\ \hat{S}_x &\rightarrow \hat{S}_x, & \hat{S}_y &\rightarrow \hat{S}_y, & \hat{S}_z &\rightarrow \hat{S}_z, \end{aligned} \quad (16)$$

if the origin point of z -axis is set at the mid-plane of the quantum well. Applying the space inversion transformation (16) to Eq. (13), we have

$$\langle \hat{S}_\alpha \rangle = \chi_{\alpha\beta} E_\beta \rightarrow \langle \hat{S}_\alpha \rangle = -\chi_{\alpha\beta} E_\beta, \quad (17)$$

whereby $\chi_{\alpha\beta} = -\chi_{\alpha\beta}$. This implies that no CISP appears when the inversion symmetry exists in the system. So the asymmetrical potential V_a is crucial for the CISP.

In the presence of an asymmetrical potential V_a , the Hamiltonian (1) is invariant versus the rotation along z -axis with $\frac{\pi}{2}$ in both the real space and the spin space,

$$\begin{aligned} x &\rightarrow y, & y &\rightarrow -x, & z &\rightarrow z, \\ \hat{S}_x &\rightarrow \hat{S}_y, & \hat{S}_y &\rightarrow -\hat{S}_x, & \hat{S}_z &\rightarrow \hat{S}_z. \end{aligned} \quad (18)$$

With the above transformations (18), Eq. (13) will give

$$\langle \hat{S}_x \rangle = \chi_{xy} E_y \rightarrow \langle \hat{S}_y \rangle = -\chi_{xy} E_x, \quad (19)$$

$$\langle \hat{S}_x \rangle = \chi_{xx} E_x \rightarrow \langle \hat{S}_y \rangle = \chi_{xx} E_y. \quad (20)$$

Combined with $\langle \hat{S}_y \rangle = \chi_{yx} E_x$ and $\langle \hat{S}_y \rangle = \chi_{yy} E_y$, we get

$$\chi_{xy} = -\chi_{yx}, \quad (21)$$

$$\chi_{xx} = \chi_{yy}, \quad (22)$$

which are direct consequence of the rotation symmetry along the z -axis.

III. ANALYTICAL RESULTS FOR CISP IN 2DHG

In the low hole density regime an effective Hamiltonian can be obtained by projecting the Hamiltonian (1) into the subspace spanned by the lowest heavy hole states, which, by using the truncation approximation and projection perturbation method,^{35,36,37,41,42,43,44,45} is reduced to the widely used k -cubic Rashba model. More importantly, the corresponding spin operators in the subspace will be obtained properly, and the ESS of 2DHG with the impurity vertex correction will be worked out. Then we will compare and contrast the different behaviors of the CISP in the 2DEG and 2DHG in this Section.

A. k -cubic Rashba Model

To obtain an approximate analytical expression, we take the following procedure. First we expand a hole state in terms of 8 basis wave functions associated with $|n, \lambda_h\rangle$ ($n = 1, 2$ and $\lambda_h = \frac{3}{2}, \frac{1}{2}, -\frac{1}{2}, -\frac{3}{2}$) (Eq. 12). Then for a given \mathbf{k} , we may express the Hamiltonian (1) in

terms of an 8×8 matrix, which by the perturbation procedure can be further projected into the subspace spanned by the $|1, \frac{3}{2}\rangle$ and $|1, -\frac{3}{2}\rangle$ states. Thus we obtain a 2×2 matrix as (See Appendix A for details),

$$\hat{H}_{k^3} = \frac{\hbar^2 k^2}{2m_h} + i\alpha(k_-^3 \sigma_+ - k_+^3 \sigma_-), \quad (23)$$

where the Pauli matrix $\sigma_{\pm} \equiv \frac{1}{2}(\sigma_x \pm i\sigma_y)$, the effective mass is renormalized into

$$m_h = m_0 \left(\gamma_1 + \gamma_2 - \frac{256\gamma_2^2}{3\pi^2(3\gamma_1 + 10\gamma_2)} \right)^{-1}, \quad (24)$$

and the k -cubic Rashba coefficient

$$\alpha = \frac{512eFL_z^4\gamma_2^2}{9\pi^6(3\gamma_1 + 10\gamma_2)(\gamma_1 - 2\gamma_2)}. \quad (25)$$

Note that Eq. (23) is just the k -cubic Rashba model, in which the Rashba coefficient α is proportional to asymmetrical potential strength F , in agreement with the results by Winkler.³⁵ We can rewrite the k -cubic Rashba Hamiltonian (23) as

$$\hat{H}_{k^3} = \varepsilon(\mathbf{k}) + \sum_{i=x,y,z} d_i(\mathbf{k})\sigma_i, \quad (26)$$

where $d_x = \alpha k_y(3k_x^2 - k_y^2)$, $d_y = \alpha k_x(3k_y^2 - k_x^2)$, $d_z = 0$, and $\varepsilon(\mathbf{k}) = \frac{\hbar^2 k^2}{2m_h}$. The eigenvalue associated with the spin index μ ($\mu = \pm 1$) is

$$E_{\mu}(k) = \varepsilon(\mathbf{k}) + \mu\alpha k^3, \quad (27)$$

with the eigenfunction

$$\psi_{\mathbf{k}\mu}(\mathbf{r}) = \frac{e^{i\mathbf{k}\cdot\mathbf{r}}}{\sqrt{2A_S}} \begin{pmatrix} i \\ \mu e^{i3\theta} \end{pmatrix}, \quad (28)$$

where A_S is the area of the system.

The k -cubic Rashba model has been widely used to study the spin Hall effect in 2DHG,^{32,33,34} however, no sufficient attention has been paid to the corresponding spin operators. For example, although Hamiltonian (23) is written in terms of the Pauli matrices σ , the σ matrix is no longer related to the spin directly. The correct spin operators in the k -cubic Rashba model, as described in Appendix A, are expressed as

$$\tilde{S}_x = \begin{pmatrix} -S_0 k_y & S_1 k_-^2 \\ S_1 k_+^2 & -S_0 k_y \end{pmatrix}, \quad (29)$$

$$\tilde{S}_y = \begin{pmatrix} S_0 k_x & -iS_1 k_-^2 \\ iS_1 k_+^2 & S_0 k_x \end{pmatrix}, \quad (30)$$

$$\tilde{S}_z = \frac{3}{2}\sigma_z, \quad (31)$$

in which

$$S_0 = \frac{512\gamma_2 L_z^4 e F m_0}{9\pi^6 \hbar^2 (3\gamma_1 + 10\gamma_2)(\gamma_1 - 2\gamma_2)}, \quad (32)$$

$$S_1 = \left[\frac{3}{4\pi^2} - \frac{256\gamma_2^2}{3\pi^4(3\gamma_1 + 10\gamma_2)^2} \right] L_z^2. \quad (33)$$

Clearly, the coefficient S_0 and the Rashba coefficient α have the same dependence on F and L_z , thus we have

$$S_0 = \frac{\alpha m_0}{\hbar^2 \gamma_2}. \quad (34)$$

S_z is related to σ_z , while $S_x(S_y)$ consists of two parts: the diagonal part linear in $k_y(k_x)$ and the non-diagonal part quadratic in k_{\pm} . The diagonal part, which relates the wave vector $k_y(k_x)$ with $S_x(S_y)$, will give the main contribution to CISP. The velocity operator in the k -cubic Rashba model can also be obtained by the projection technique,

$$\tilde{v}_x = \frac{\hbar k_x}{m_h} + \frac{3i\alpha}{\hbar}(k_-^2 \sigma_+ - k_+^2 \sigma_-), \quad (35)$$

which is consistent with the relation $\tilde{v}_x = \frac{1}{\hbar} \partial H_{k^3} / \partial k_x$.

B. Impurity Vertex correction

Now, we calculate the ESS in the framework of the linear response theory based on k -cubic Rashba model (23). In doing this we take the vertex correction of impurities into account. The free retarded Green function has the form,

$$G_0^R(\mathbf{k}, E) = \frac{E - \varepsilon(\mathbf{k}) + \sum_i d_i \sigma_i}{(E - E_+ + i\eta)(E - E_- + i\eta)}, \quad (36)$$

where η is an infinitesimal positive number. We assume impurities to be distributed randomly in the form $V_r(\mathbf{r}) = V_0 \sum_i \delta(\mathbf{r} - \mathbf{R}_i)$, where V_0 is the strength. With the Born approximation, the self-energy, diagonal in the spin space, is given by

$$Im[\Sigma_0^R(\mathbf{k}, E)] = \frac{n_i V_0^2 \pi}{2} (D_+ + D_-), \quad (37)$$

where n_i is the impurity density, and the density of states for two spin-split branches of the HH1 subband reads

$$D_{\pm}(k) = \frac{m_h}{2\pi\hbar^2} \left| 1 \pm \frac{3m_h\alpha k}{\hbar^2} \right|^{-1}. \quad (38)$$

So the configuration-averaged Green function is given by

$$G^R(\mathbf{k}, E) = \frac{E - \varepsilon(k) + i\Gamma_0 + \sum_i d_i \sigma_i}{(E - E_+ + i\Gamma_0)(E - E_- + i\Gamma_0)}, \quad (39)$$

where $\Gamma_0 = -Im[\Sigma_0^R(\mathbf{k}, E)] = \frac{\hbar}{2\tau}$ and τ is the momentum relaxation time. In the ladder approximation, the Strada-Smrcka formula (15) for the ESS χ will reduce to

$$\chi_{\alpha\beta} = e\hbar \int \frac{dE}{2\pi} \left(-\frac{\partial f(E)}{\partial E} \right) \int \frac{d^2k}{(2\pi)^2} Tr \left[\tilde{S}_{\alpha} G^R \Upsilon_{\beta} G^A \right], \quad (40)$$

where $\tilde{\mathbf{S}}$ is given by Eqs.(29)-(31) and the vertex function $\Upsilon_{\beta}(\mathbf{k})$ satisfies the self-consistent equation³⁸

$$\Upsilon_{\beta} = \tilde{v}_{\beta} + n_i V_0^2 \int \frac{d^2k}{(2\pi)^2} G^R(\mathbf{k}, E) \Upsilon_{\beta} G^A(\mathbf{k}, E). \quad (41)$$

Suppose the electric field is along the x-direction, we solve the vertex function Υ_x iteratively, and get the first-order

correction to Υ_x as

$$\Delta\Upsilon_x^{(1)} = n_i V_0^2 \int \frac{kdkd\theta}{(2\pi)^2} \frac{\begin{pmatrix} E - \varepsilon(\mathbf{k}) & i\alpha k_-^3 \\ -i\alpha k_+^3 & E - \varepsilon(\mathbf{k}) \end{pmatrix} \begin{pmatrix} \frac{\hbar k_x}{m_h} & \frac{3i\alpha}{\hbar} k_-^2 \\ -\frac{3i\alpha}{\hbar} k_+^2 & \frac{\hbar k_x}{m_h} \end{pmatrix} \begin{pmatrix} E - \varepsilon(\mathbf{k}) & i\alpha k_-^3 \\ -i\alpha k_+^3 & E - \varepsilon(\mathbf{k}) \end{pmatrix}}{((E - E_+)^2 + \Gamma_0^2)((E - E_-)^2 + \Gamma_0^2)}. \quad (42)$$

Note that E_{\pm} and Γ_0 are independent of θ and all terms in the numerator of the integrand contain something like $\exp(\pm i\theta)$ etc., so the integral over θ from 0 to 2π in Eq.(42) vanishes. Furthermore, the higher order terms for the vertex correction vanish either, which is quite different from the vertex correction in the linear- \mathbf{k} Rashba model.⁸ The same situation occurs for Υ_y . The above results agree with the work by Schliemann and Loss.³³ The calculation of the spin polarization is straightforward, and to the lowest order in Fermi momentum k_{\pm}^F and α , only the term proportional to S_0 contributes to the spin polarization. The final result reads

$$\chi_{yx} = -\chi_{xy} = \frac{eS_0\tau m_h E_F}{\hbar^3 \pi} = S_0 n_h \frac{e\tau}{\hbar}, \quad (43)$$

$$\chi_{xx} = \chi_{yy} = 0, \quad (44)$$

where n_h is the hole density, E_F is the Fermi energy, and only the leading term in E_F is retained.

In the relaxation time approximation the longitudinal conductivity of 2DHG equals to

$$\sigma_{xx} = \frac{e^2 \tau E_F}{\hbar^2 \pi}. \quad (45)$$

Thus, combining the expressions (43) and (45), we have the ratio

$$\frac{\langle \tilde{S}_y \rangle}{\langle j_x \rangle} = \frac{\chi_{yx}}{\sigma_{xx}} = \frac{S_0 m_h}{e \hbar} = \frac{\alpha m_0 m_h}{e \hbar^3 \gamma_2}. \quad (46)$$

The formula above can be also obtained from the expression of the spin operator (30) and the velocity operator (35) by neglecting the non-diagonal part in the spin operator and the anomalous part in the velocity operator, i.e. $\tilde{S}_y \approx S_0 k_x$ and $j_x \approx e \hbar k_x / m_h$. Obviously, this ratio depends only on the material parameters, but not on the impurity scattering nor the carrier density in the low density limit. Meanwhile, since both the current and spin polarization can be measured experimentally, the relation (46) may be invoked to obtain the k -cubic Rashba coefficient α experimentally.

C. Comparing CISP of 2DHG and 2DEG

The CISP of 2DHG manifests itself several features different from that of 2DEG. To illustrate this, let's first

take a look at the CISP of 2DEG. The electric spin susceptibility is given by $\chi_{yx} = 2e\tau\alpha_e m_e / \hbar^2$, where m_e is the effective mass of electron and α_e is the linear Rashba coefficient. As shown by Inoue *et al.*⁸, the vertex correction due to the linear Rashba spin splitting is non-trivial. With the longitudinal conductivity of 2DEG $\sigma_{xx} = e^2 \tau E_F / (\hbar^2 \pi)$, we find the ratio of spin polarization to the current for the 2DEG is

$$\frac{\langle S_y^{(e)} \rangle}{\langle j_x \rangle} = \frac{\chi_{yx}}{\sigma_{xx}} = \frac{2\pi m_e \alpha_e}{e E_F}. \quad (47)$$

Compared with (46), we find the CISP of 2DEG is inversely proportional to Fermi energy. This means the ratio for 2DEG decreases for heavier doping. This different Fermi-energy dependence stems from the different types of spin orientation for 2DEG and 2DHG.

The spin orientation, which is the expectation value of spin operator \mathbf{S} for an eigenstate, is given by

$$\langle k\mu | \tilde{S}_x | k\mu \rangle = -S_0 k \sin \theta + \mu k^2 S_1 \sin \theta, \quad (48)$$

$$\langle k\mu | \tilde{S}_y | k\mu \rangle = S_0 k \cos \theta - \mu k^2 S_1 \cos \theta, \quad (49)$$

$$\langle k\mu | \tilde{S}_z | k\mu \rangle = 0, \quad (50)$$

for 2DHG, and

$$\langle k\mu | S_x^{(e)} | k\mu \rangle = -\mu \sin \theta, \quad (51)$$

$$\langle k\mu | S_y^{(e)} | k\mu \rangle = \mu \cos \theta, \quad (52)$$

$$\langle k\mu | S_z^{(e)} | k\mu \rangle = 0, \quad (53)$$

for 2DEG. In the following, we take $\langle \mathbf{S} \rangle_{k\mu}$ as short for the spin orientation above. Eqs. (51) and (52) show that spin orientation for 2DEG depends on the spin index μ , which has opposite values for the two spin-splitting states. But for 2DHG, the first term in Eqs. (48) and (49) is independent of the spin index μ . Hence, when k is small, this spin-index-independent term will dominate over the k^2 -term, leading to the same spin orientation for the hole state with opposite μ . This is quite different from the electron case. An interesting question may be raised: why the holes with opposite μ have the same spin orientation? In the following, we will analyze this problem and try to find the origin of this particular spin orientation for 2DHG.

Let's first have a look at the electron case. Due to the spin-orbit coupling and inversion asymmetry, two-fold degeneracy of a subband is lifted. For a given k ,

we denote two spin-split states as $|+\rangle = \cos\frac{\theta}{2}e^{-i\phi}|\frac{1}{2}\rangle_z + \sin\frac{\theta}{2}|\frac{1}{2}\rangle_z$ and $|-\rangle = -\sin\frac{\theta}{2}e^{-i\phi}|\frac{1}{2}\rangle_z + \cos\frac{\theta}{2}|\frac{1}{2}\rangle_z$, where $|\pm\frac{1}{2}\rangle_z$ are the eigenstates of σ_z . It is easy to verify that $|+\rangle$ and $|-\rangle$ have the opposite spin orientation, namely $\langle +|\vec{\sigma}|+\rangle = -\langle -|\vec{\sigma}|-\rangle$.

Similar to 2DEG, two spin-split hole states in the subspace $|\pm\frac{3}{2}\rangle$ can be constructed as $|+\rangle = \cos\frac{\theta}{2}e^{-i\phi}|\frac{3}{2}\rangle + \sin\frac{\theta}{2}|\frac{3}{2}\rangle$ and $|-\rangle = -\sin\frac{\theta}{2}e^{-i\phi}|\frac{3}{2}\rangle + \cos\frac{\theta}{2}|\frac{3}{2}\rangle$. By Eqs. (8) and (9), we can verify the matrix elements of \hat{S}_x and \hat{S}_y between $|\frac{3}{2}\rangle$ and $|\frac{3}{2}\rangle$ vanish, and $\langle \pm|\hat{S}_x|\pm\rangle = \langle \pm|\hat{S}_y|\pm\rangle = 0$. This indicates that in the subspace $|\pm\frac{3}{2}\rangle$, any superposition of $|\pm\frac{3}{2}\rangle$ will not give rise to the spin orientation along the x- or y-direction. Thus it is necessary to take the higher order perturbation into account, in particular the perturbation from coupling between $|\pm\frac{3}{2}\rangle$ and $|\pm\frac{1}{2}\rangle$.

Now we give the outline on the origin of the hole spin orientation by the perturbation procedure (more systematic method can be found in Appendix A). Suppose the $HH1\pm$ states $\Psi_{hh,\pm}$ can be expanded as

$$\Psi_{hh,\pm} = \Psi_{hh,\pm}^{(0)} + \Psi_{hh,\pm}^{(1)} + \Psi_{hh,\pm}^{(2)} + \dots, \quad (54)$$

where $\Psi_{hh,\pm}^{(i)}$ denotes the i th-order perturbed wave function. With the basis $|n, \lambda_h\rangle$ [Eq. (12)] and the 0th-order term

$$\Psi_{hh,\pm}^{(0)} = |1, \pm\frac{3}{2}\rangle, \quad (55)$$

we have the first-order correction as

$$\begin{aligned} \Psi_{hh,+}^{(1)} &= \frac{|2, \frac{1}{2}\rangle\langle 2, \frac{1}{2}|R^\dagger|1, \frac{3}{2}\rangle}{E_{1,\frac{3}{2}} - E_{2,\frac{1}{2}}} + \frac{|1, -\frac{1}{2}\rangle\langle 1, -\frac{1}{2}|T^\dagger|1, \frac{3}{2}\rangle}{E_{1,\frac{3}{2}} - E_{1,-\frac{1}{2}}} \\ &+ \frac{|2, \frac{3}{2}\rangle\langle 2, \frac{3}{2}|V_a|1, \frac{3}{2}\rangle}{E_{1,\frac{3}{2}} - E_{2,\frac{3}{2}}}, \end{aligned} \quad (56)$$

$$\begin{aligned} \Psi_{hh,-}^{(1)} &= \frac{|1, \frac{1}{2}\rangle\langle 1, \frac{1}{2}|T|1, -\frac{3}{2}\rangle}{E_{1,-\frac{3}{2}} - E_{1,\frac{1}{2}}} - \frac{|2, -\frac{1}{2}\rangle\langle 2, -\frac{1}{2}|R|1, -\frac{3}{2}\rangle}{E_{1,-\frac{3}{2}} - E_{2,-\frac{1}{2}}} \\ &+ \frac{|2, -\frac{3}{2}\rangle\langle 2, -\frac{3}{2}|V_a|1, -\frac{3}{2}\rangle}{E_{1,-\frac{3}{2}} - E_{2,-\frac{3}{2}}}, \end{aligned} \quad (57)$$

and the second-order correction reads

$$\begin{aligned} \Psi_{hh,+}^{(2)} &= \frac{|1, \frac{1}{2}\rangle\langle 1, \frac{1}{2}|V_a|2, \frac{1}{2}\rangle\langle 2, \frac{1}{2}|R^\dagger|1, \frac{3}{2}\rangle}{(E_{1,\frac{3}{2}} - E_{1,\frac{1}{2}})(E_{1,\frac{3}{2}} - E_{2,\frac{1}{2}})} \\ &+ \frac{|1, \frac{1}{2}\rangle\langle 1, \frac{1}{2}|R^\dagger|2, \frac{3}{2}\rangle\langle 2, \frac{3}{2}|V_a|1, \frac{3}{2}\rangle}{(E_{1,\frac{3}{2}} - E_{1,\frac{1}{2}})(E_{1,\frac{3}{2}} - E_{2,\frac{3}{2}})} + \dots, \end{aligned} \quad (58)$$

and

$$\begin{aligned} \Psi_{hh,-}^{(2)} &= -\frac{|1, -\frac{1}{2}\rangle\langle 1, -\frac{1}{2}|V_a|2, -\frac{1}{2}\rangle\langle 2, -\frac{1}{2}|R|1, -\frac{3}{2}\rangle}{(E_{1,-\frac{3}{2}} - E_{1,-\frac{1}{2}})(E_{1,-\frac{3}{2}} - E_{2,-\frac{1}{2}})} \\ &- \frac{|1, -\frac{1}{2}\rangle\langle 1, -\frac{1}{2}|R|2, -\frac{3}{2}\rangle\langle 2, -\frac{3}{2}|V_a|1, -\frac{3}{2}\rangle}{(E_{1,-\frac{3}{2}} - E_{1,-\frac{1}{2}})(E_{1,-\frac{3}{2}} - E_{2,-\frac{3}{2}})} + \dots \end{aligned} \quad (59)$$

Here E_{n,λ_h} stands for the eigenenergy of the state $|n, \lambda_h\rangle$. From Eqs. (8) and (9), we can see when $n = 1$ the only nonvanishing terms are $\langle 1, \frac{3}{2}|\hat{S}_{x(y)}|1, \frac{1}{2}\rangle$ and $\langle 1, -\frac{3}{2}|\hat{S}_{x(y)}|1, -\frac{1}{2}\rangle$. Up to the second-order perturbation, two types of terms can contribute to $\langle \Psi_{hh,\pm}|\hat{S}_{x(y)}|\Psi_{hh,\pm}\rangle$.

The first type stems from the first-order perturbation by the T -operator in the Luttinger Hamiltonian [Eq. (3)], which couples $|1, -\frac{1}{2}\rangle$ ($|1, \frac{1}{2}\rangle$) to $|1, -\frac{3}{2}\rangle$ ($|1, \frac{3}{2}\rangle$) [the second term in Eq. (56) or (57)]. So the matrix element $\langle \Psi_{hh,+}|\hat{S}_x|\Psi_{hh,-}\rangle$ equals to

$$\langle \Psi_{hh,+}^{(0)}|\hat{S}_x|\Psi_{hh,-}^{(1)}\rangle + \langle \Psi_{hh,+}^{(1)}|\hat{S}_x|\Psi_{hh,-}^{(0)}\rangle = \frac{3}{4\pi^2}L_z^2k_-^2. \quad (60)$$

It is obvious that the above formula is just the off-diagonal element in \hat{S}_x matrix [Eq. (29)] with the first term in square bracket of S_1 [Eq. (33)] retained. This gives the quadratic- k dependence of the spin orientation shown as the second term in Eq. (48).

The second type comes from joint action of the R in Luttinger Hamiltonian and the asymmetrical potential V_a [See Eqs. (58) and (59)]. The second-order perturbation contributes to $\langle \Psi_{hh,+}|\hat{S}_x|\Psi_{hh,+}\rangle$ with

$$\begin{aligned} &\langle \Psi_{hh,+}^{(0)}|\hat{S}_x|\Psi_{hh,+}^{(2)}\rangle + \langle \Psi_{hh,+}^{(2)}|\hat{S}_x|\Psi_{hh,+}^{(0)}\rangle \\ &+ \langle \Psi_{hh,+}^{(1)}|\hat{S}_x|\Psi_{hh,+}^{(1)}\rangle \\ &= -\frac{512\gamma_2L_z^4eFm_0k_y}{9\pi^6\hbar^2(3\gamma_1 + 10\gamma_2)(\gamma_1 - 2\gamma_2)}. \end{aligned} \quad (61)$$

This term is just the diagonal element in Eq. (29), which leads to the first term in Eq. (48) and is responsible for the identical spin orientation for two spin splitting hole states in small k regime.

The spin splitting between $HH\pm$ depends on the coupling between $|1, \frac{3}{2}\rangle$ and $|1, -\frac{3}{2}\rangle$ through higher-order perturbation. Different from the electron case, the direct coupling will not cause the x-direction or y-direction spin orientation. Instead, it results from the coupling between $|1, \frac{3}{2}\rangle$ ($|1, -\frac{3}{2}\rangle$) and $|1, \frac{1}{2}\rangle$ ($|1, -\frac{1}{2}\rangle$). For two LH1 states, denoted as $\Psi_{lh,\pm}$, such coupling will lead to the spin orientations of $\Psi_{lh,+}$ opposite to $\Psi_{hh,+}$, and that of $\Psi_{lh,-}$ opposite to $\Psi_{hh,-}$. Thus the total spin orientation of the 2DHG is conserved, though $\Psi_{hh,+}$ and $\Psi_{hh,-}$ have the same spin orientation in the low hole density regime.

IV. NUMERICAL RESULTS FOR CISP IN 2DHG

Based on the calculated eigenstates and eigenenergies of the total Hamiltonian (1), in this Section we will work out the spin polarization by using the Bastin version of Kubo formula (14) in the relaxation time approximation. Of course the validity of such approximation depends on the vanishing vertex correction as mentioned above.

Our numerical results with an expanded basis set of N basis functions (N is much larger than 8 used in last Section) shows that for a quantum well with infinitely high potential barrier, when increasing N , the eigenenergies converge to the exact solutions formulated by Huang *et. al.*⁴⁶ very quickly. For example, for the quantum well with width $L_z = 83\text{\AA}$, several lowest hole subbands obtained with $N = 20$ are almost identical to the exact results. Even for $N = 8$, the dispersion of the lowest heavy and light hole subbands is in good agreement with the exact results, demonstrating the validity of the truncation procedure in last Section and Appendix A. Fig. 1 plot the dispersion curves and spin splitting of hole subbands in the quantum well in the presence of an electric field. Due to the heavy and light hole mixture effect, the energy minimum of the lowest light hole subband, marked by B in the Figure, deviates from the Γ -point significantly.

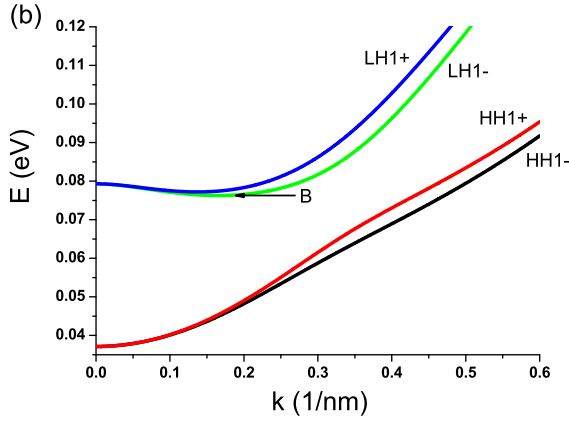


FIG. 1: (Color online) Dispersion relation for a quantum well with infinite barrier in an electric field. $HH1\pm$ and $LH1\pm$ denote two lowest heavy- and light- hole subbands, respectively. The parameters for calculation are taken as: the well width $L_z = 83\text{\AA}$, the field strength $F = 50\text{ kV/cm}$, $\gamma_1 = 7$ and $\gamma_2 = 1.9$

For the electric spin susceptibility, we calculate χ_{yx} only, because $\chi_{xx} = \chi_{yy} = 0$ and $\chi_{xy} = \chi_{yx}$ as indicated by Eq. (21). After some algebra, we can divide ESS in Eq.(14) into an intra-subband part χ_{yx}^I and an inter-subband part χ_{yx}^{II} , which are expressed respectively as

$$\chi_{yx}^I = \frac{e\hbar}{2\pi} \int \frac{d^2k}{(2\pi)^2} \sum_{\nu} \langle k\nu | \hat{S}_y | k\nu \rangle \langle k\nu | \hat{v}_x | k\nu \rangle \frac{A_{\nu}^2}{2}, \quad (62)$$

$$\chi_{yx}^{II} = \frac{e\hbar}{2\pi} \int \frac{d^2k}{(2\pi)^2} \sum_{\nu > \nu'} \Re(\langle k\nu | \hat{S}_y | k\nu' \rangle \langle k\nu' | \hat{v}_x | k\nu \rangle) A_{\nu} A_{\nu'}. \quad (63)$$

Here \Re denotes the real part, and ν and ν' stand for

the hole subband. In relaxation time approximation, the spectral function A_{ν} can be expressed as

$$A_{\nu} = \frac{2\eta}{((E - E_{\nu})^2 + \eta^2)^2}, \quad (64)$$

where $\eta = \frac{\hbar}{2\tau}$.

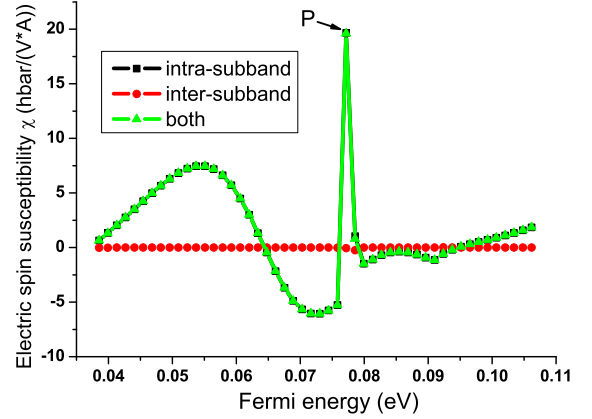


FIG. 2: (Color online) The calculated ESS for the intra-subband term (black square line), inter-subband term (red circle line), and their sum (green triangle line). The scattering induced broadening η is taken as $1.65 \times 10^{-5} \text{ eV}$, corresponding to the relaxation time $\tau = 2 \times 10^{-11} \text{ s}$. The spin polarization peak marked with P corresponds to the energy minimum of the lowest light hole subband marked as B in Fig. 1.

A typical curve for the CISP is plotted in Fig. 2. The main contribution to CISP comes from the intra-subband term, which can be understood by Eq. (63). In the limit $\eta \rightarrow 0$, the spectral function A_{ν} tends to be the delta-function $2\pi\delta(E - E_{\nu})$, making the inter-subband term $A_{\nu}A_{\nu'}$ to vanish except for an accidental degeneracy. Several features in Fig. 2 are worth pointing out. First, in low doping regime where only $HH1\pm$ states near Γ point are occupied, spin polarization exhibits a linear dependence on the Fermi energy. Second, with the hole density increased, the spin polarization increases at first, then decrease after reaching a maximum value, and even changes its sign when the hole density is large enough. Third, when the doping is so heavy that the light hole subband is occupied, a sharp peak for the spin polarization may be observed as marked as P in Fig. 2.

To understand these features, we turn back to Eq. (62), as main contribution to the spin polarization stems from this intra-subband term. Based on numerical results as well as Eq. (49), we adopt a function $J_{\nu}(k)$ to express the amplitude of the spin orientation associated with the subband ν , i.e.

$$(S_y)_{\nu\nu} = J_{\nu}(k) \cos\theta.$$

Then, with

$$(v_x)_{\nu\nu} = \frac{1}{\hbar} \frac{\partial E_\nu}{\partial k_x} = \frac{1}{\hbar} \frac{\partial E_\nu(k)}{\partial k} \cos \theta,$$

and

$$A_\nu^2 = \frac{4\pi\tau}{\hbar} \delta(E_F - E_\nu),$$

we rewrite Eq. (62) as

$$\chi_{yx} = \frac{e\tau}{4\pi\hbar} \sum_\nu k_\nu^F J_\nu(k_\nu^F), \quad (65)$$

where k_ν^F is the Fermi momentum with the hole subband ν .

In the k -cubic Rashba model, in which only the lowest heavy hole subband $HH1\pm$ is concerned, up to the first-order in α , the Fermi momentum can be expressed as $k_\mu^F = \frac{\sqrt{2m_h E_F}}{\hbar} - \mu \frac{2\alpha m_h^2 E_F}{\hbar^4}$. Combined with Eq.(49), we obtain

$$\chi_{yx} = \frac{e\tau m_h S_0 E_F}{\pi \hbar^3} + \frac{3e\tau m_h^3 \alpha S_1 E_F^2}{\pi \hbar^7}. \quad (66)$$

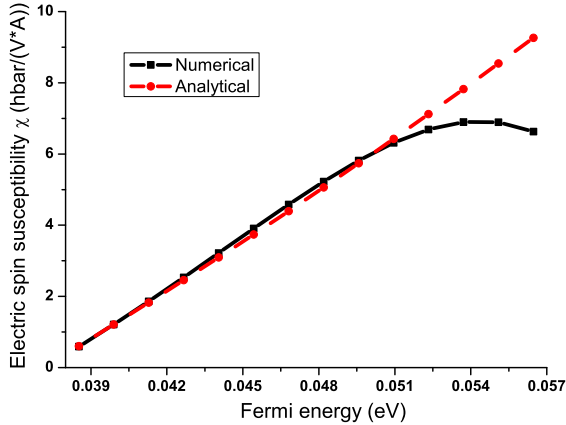


FIG. 3: (Color online) Numerically calculated ESS as functions of Fermi energy (black-square-line) compared with the analytical results (red-circle-line).

The first term on the right hand side of Eq. (66), resulting from the spin-independent part, is identical to Eq. (43); while the second term, proportional to E_F^2 , can be safely ignored in the low density regime. As shown in Fig. 3, the analytical results of the electric spin susceptibility (Eq. 66) agree well with the numerical ones, demonstrating the applicability of k -cubic Rashba model (23) in low doping regime. However, for higher hole density, numerical results show a drop of the χ due to the heavy and light hole mixing effect, which is certainly beyond the simple k -cubic Rashba model.

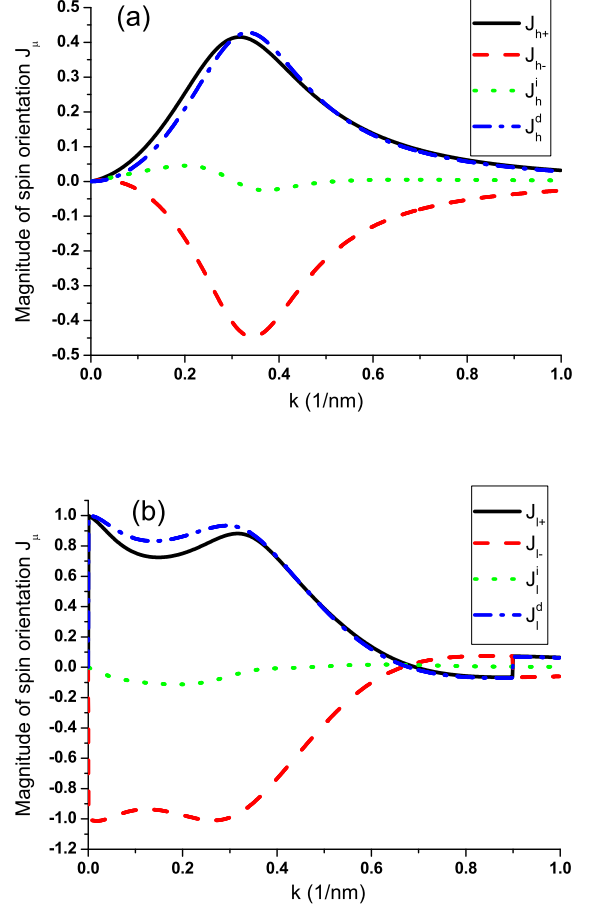


FIG. 4: (Color online) The magnitude of the spin orientation for the lowest heavy hole subband (a) and the lowest light hole subband (b). In (a), the black solid line and red dashed line represent J_{h+} and J_{h-} , respectively; while the green dotted line and blue dashed dotted line denote the spin-independent part J_h^i and dependent part J_h^d , respectively. The same notions are also applied to (b).

For numerical results, similar to the derivation above, we may divide J_ν into a spin-dependent part and a spin-independent one, namely, $J_{\nu\mu} = J_\nu^i + \mu J_\nu^d$. Then the ESS can be expressed as

$$\chi_{yx} = \chi_{yx}^i + \chi_{yx}^d, \quad (67)$$

in which the spin-independent and dependent part respectively reads

$$\chi_{yx}^i = \frac{e\tau}{2\pi\hbar} \sum_\nu J_\nu^i \frac{k_{\nu+}^F + k_{\nu-}^F}{2}, \quad (68)$$

$$\chi_{yx}^d = \frac{e\tau}{2\pi\hbar} \sum_\nu J_\nu^d \frac{k_{\nu+}^F - k_{\nu-}^F}{2}. \quad (69)$$

Obviously, χ_{yx}^i depends on the average of Fermi

wavenumbers, while χ_{yx}^d depends on the Fermi wavenumber difference between two spin-split branches. In most cases, owing to the fact that the spin splitting is small compared with the Fermi energy, χ_{yx}^i will dominate the spin polarization. In Fig. 4(a), we plot the magnitude of spin orientation associated with the subband $HH1\pm$, denoted by $J_{h\pm}$, and the corresponding spin-dependent part, J_h^d , and independent part J_h^i . They are related through $J_h^d = (J_{h+} - J_{h-})/2$ and $J_h^i = (J_{h+} + J_{h-})/2$. Fig. 4 indicates that for most values of k J_h^d is larger than J_h^i . Compared to the intra-subband contribution in Fig. 2, the spin-independent magnitude of the spin polarization J_h^i [green-dotted line in Fig. 4(a)] has similar behavior: first increasing linearly with k , then decreasing with k increased, and even changing the sign for larger k .

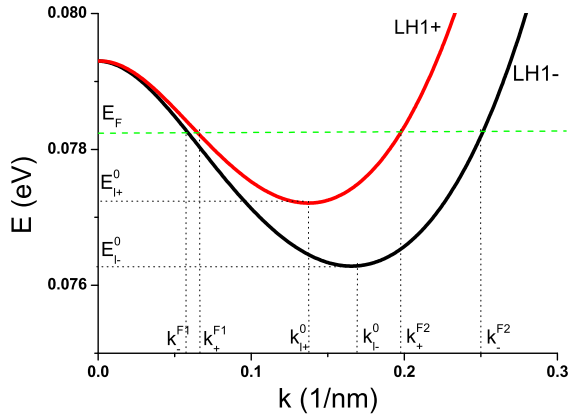


FIG. 5: (Color online) Dispersion relation of the lowest light hole subband $LH1\pm$.

A pronounced peak of CISP may appear when the Fermi energy just crosses the bottom of the lowest light hole subband $LH1-$. As amplified in Fig. 5, in the dispersion relation of the subband $LH1\pm$, the wave numbers $k_{l\pm}^0$ corresponding to the energy minimum $E_{l\pm}^0$ deviate from the $k = 0$ point significantly. Around the energy minimum the energy dispersion can be approximated as $E_{l\mu}(k) = E_{l\mu}^0 + \frac{1}{2} \frac{\partial^2 E_{l\mu}(k)}{\partial k^2} (k - k_{l\mu}^0)^2$. Assuming the above energy dispersion and a constant magnitude of $J_{l\mu}$, we obtain

$$\chi_{yx}^{\mu} = \frac{e\tau}{2\pi\hbar} k_{l\mu}^0 J_{l\mu}(k_{l\mu}^0), \quad (70)$$

where $k_{l\mu}^0 \simeq (k_{\mu}^{F1} + k_{\mu}^{F2})/2$, and k_{\pm}^{F1} and k_{\pm}^{F2} respectively denote two different Fermi wave numbers for $LH1\pm$ (Fig. 5). By Eq. (70) and Fig. 4(b), we can see since J_{l+} and J_{l-} are large in the absolute value but almost opposite in the sign, when $E_{l+}^0 > E_F > E_{l-}^0$, a large spin polarization $e\tau k_{l-}^0 J_{l-}/(2\pi\hbar)$ is expected; on the other hand, when $E_F > E_{l+}^0 > E_{l-}^0$, the contributions of $LH1\pm$ to the spin

polarization cancel each other to some extent, resulting in

$$\chi_{yx} = \frac{e\tau}{2\pi\hbar} [(k_{l-}^0 + k_{l+}^0)J_{l+}^i + (k_{l+}^0 - k_{l-}^0)J_{l+}^d]. \quad (71)$$

As J_{l+}^i is much smaller than J_{l+}^d or $J_{l\pm}$, and $k_{l+}^0 \approx k_{l-}^0$, both terms in Eq. (71) are small compared to the case when only $LH-$ is occupied. Apparently, the peak width depends on the spin splitting between $LH-$ and $LH+$.

The temperature dependence of the peak is plotted in Fig. 6. Near the polarization peak, if we only take into account $LH1\pm$, ESS is expressed by

$$\chi_{yx} = \frac{e\tau}{2\pi\hbar} \sum_{\mu} f(E_{l\mu}^0) k_{l\mu}^0 J_{l\mu}(k_{l\mu}^0). \quad (72)$$

At zero temperature, the Fermi distribution function $f(E)$ becomes the step-function $\theta(E_f - E)$, which reproduces the above analysis. At finite temperature T , if we approximate $k_{l\mu}^0 J_{l\mu}(k_{l\mu}^0) \simeq \mu k_{l\mu}^0 J_{l\mu}$, and expand the Fermi distribution function at large $k_B T$ as $f(E) = \frac{1}{2} (1 - \frac{E - E_F}{2k_B T})$ (k_B is Boltzmann constant), then Eq.(72) reduces to

$$\chi_{yx} = \frac{e\tau k_{l+}^0 J_{l+} E_{l+}^0 - E_{l-}^0}{2\pi\hbar 4k_B T}. \quad (73)$$

So ESS is proportional to the ratio of the spin splitting of the $LH1$ subband, $E_{l+}^0 - E_{l-}^0$, to thermal energy $k_B T$. When $k_B T$ is much larger than the spin splitting, this pronounced spin polarization peak will smear out.

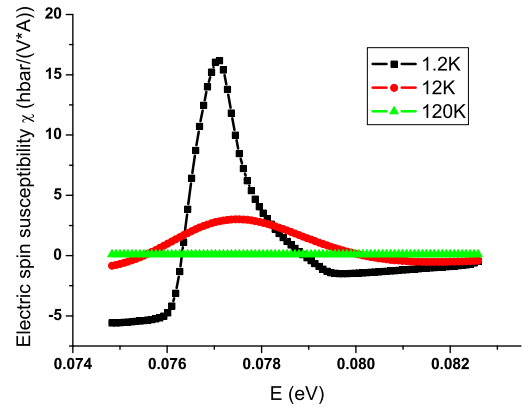


FIG. 6: (Color online) The spin polarization peak at three different temperatures, 1.2K, 12K and 120K.

Now let's estimate the magnitude of the averaged CISP. In the k -cubic Rashba model with an applied field $F = 50kV/cm$, Eq.(32) gives $S_0 = 2.74\text{\AA}$ for $L_z = 83\text{\AA}$ and $S_0 = 5.77\text{\AA}$ for $L_z = 100\text{\AA}$. If typical relaxation time τ is taken to be $2 \times 10^{-11}s$ and an in-plane electric field strength $E_0 = 10V/cm$, the Fermi sphere will be shifted by $\Delta k = eE_0\tau/\hbar = 3 \times 10^{-3}\text{\AA}^{-1}$. Substituting

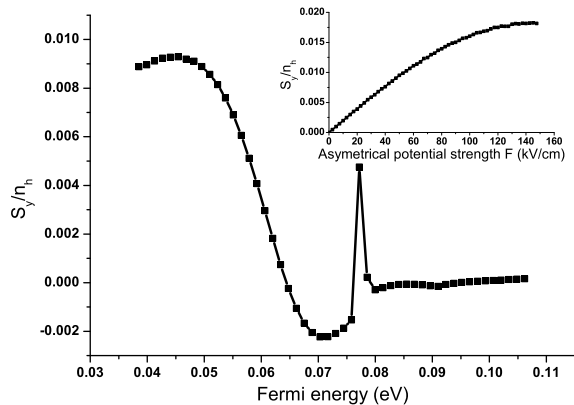


FIG. 7: $\frac{\langle S_y \rangle}{n_h}$ as functions of the Fermi energy. The inset: $\frac{\langle S_y \rangle}{n_h}$ as functions of applied field strength F .

the above data into Eq.(43), we obtain $\langle S_y \rangle / n_h = 0.831\%$ for $L_z = 83\text{\AA}$, and $\langle S_y \rangle / n_h = 1.75\%$ for $L_z = 100\text{\AA}$. Since S_0 is proportional to L_z^4 , the spin polarization is very sensitive to the thickness of quantum well. Hence, it is preferable to detect the CISP in a thicker quantum well experimentally. The above estimation gives the same order of magnitude for the spin polarization observed in Silov's experiment¹². In Fig. 7, we plot the averaged spin polarization $\langle S_y \rangle / n_h$ as functions of the Fermi energy and functions of the field F in the inset. The CISP is saturated about 2% when the field is enhanced.

V. SUMMARY

In conclusion, we have systematically investigate the current induced spin polarization of 2DHG in the frame of the linear response theory. We introduce the physical quantity of the electric spin susceptibility χ to describe CISP and give its analytical expression in the simplified k -cubic Rashba model. Different from the 2DEG, the CISP of 2DHG depends linearly on the Fermi energy. The difference of CISP between 2DHG and 2DEG results from the different spin orientations in the subband of carriers. We propose that k -cubic Rashba coefficient of 2DHG can be deduced from the ratio of spin polarization to the current, which is independent of the impurities or disorder effect up to the lowest order. We have also carried out numerical calculations for the CISP. The numerical results are consistent with the analytical one in low doping regime, which demonstrates the applicability of k -cubic Rashba model. With the increase of Fermi

energy, numerical results show that the spin polarization may be suppressed and even changes its sign. We predict and explain a pronounced spin polarization peak when the Fermi energy crosses over the subband bottom of the LH_- . We also discuss the possibility of measuring this spin polarization peak.

Acknowledgments

This work was supported by the Research Grant Council of Hong Kong under Grant No.: HKU 7041/07P, by the NSF of China (Grant No.10774086, 10574076), and by the Program of Basic Research Development of China (Grant No. 2006CB921500).

APPENDIX A: DERIVATION OF THE k -CUBIC RASHBA HAMILTONIAN

In this Appendix, we present the detailed derivation of the k -cubic Rashba model by means of the perturbation method.^{35,36,37,41,42,43,44,45} First we truncate the Hilbert space of the basis wave functions (12) into the subspace with only the lowest eight states $\mathcal{G}_0 = \{|n, \lambda_h\rangle, n = 1, 2; \lambda_h = \pm\frac{3}{2}, \pm\frac{1}{2}\}$. As described in the Sec. II, by comparing the lowest HH and LH subband dispersion with the exact solution, the accuracy of such truncation procedure has been verified. The truncated subspace \mathcal{G}_0 can be further cast into two sub-groups, \mathcal{G}_1 and \mathcal{G}_2 . \mathcal{G}_1 contains two lowest heavy hole states $\{|1, 3/2\rangle, |1, -3/2\rangle\}$, while \mathcal{G}_2 keeps the other six states, $\{|1, 1/2\rangle, |1, -1/2\rangle, |2, 3/2\rangle, |2, -3/2\rangle, |2, 1/2\rangle, |2, -1/2\rangle\}$. In this case, the Hamiltonian in the subspace \mathcal{G}_0 can be written in the form of block matrices as

$$H_{8 \times 8} = \begin{pmatrix} \tilde{H}_{2 \times 2} & \tilde{H}_{2 \times 6} \\ \tilde{H}_{6 \times 2} & \tilde{H}_{6 \times 6} \end{pmatrix}, \quad (\text{A1})$$

where

$$\tilde{H}_{2 \times 2} = \begin{pmatrix} P(1) & 0 \\ 0 & P(1) \end{pmatrix}, \quad (\text{A2})$$

$$\tilde{H}_{6 \times 2} = \tilde{H}_{2 \times 6}^\dagger = \begin{pmatrix} 0 & T \\ T^\dagger & 0 \\ eFG(2, 1) & 0 \\ 0 & eFG(2, 1) \\ R(2, 1)k_+ & 0 \\ 0 & -R(2, 1)k_- \end{pmatrix}, \quad (\text{A3})$$

and

$$\tilde{H}_{6 \times 6} = \begin{pmatrix} Q(1) & 0 & R(1,2)k_+ & 0 & eFG(1,2) & 0 \\ 0 & Q(1) & 0 & -R(1,2)k_- & 0 & eFG(1,2) \\ R(2,1)k_- & 0 & P(2) & 0 & 0 & T \\ 0 & -R(2,1)k_+ & 0 & P(2) & T^\dagger & 0 \\ eFG(2,1) & 0 & 0 & T & Q(2) & 0 \\ 0 & eFG(2,1) & T^\dagger & 0 & 0 & Q(2) \end{pmatrix}. \quad (\text{A4})$$

Here $P(n), Q(n), G(n, m), R(n, m)$ are given by

$$P(n) = \frac{\hbar^2}{2m_0} \left[(\gamma_1 + \gamma_2)k^2 + (\gamma_1 - 2\gamma_2)\left(\frac{n\pi}{L_z}\right)^2 \right] \quad (\text{A5})$$

$$Q(n) = \frac{\hbar^2}{2m_0} \left[(\gamma_1 - \gamma_2)k^2 + (\gamma_1 + 2\gamma_2)\left(\frac{n\pi}{L_z}\right)^2 \right] \quad (\text{A6})$$

$$G(n, m) = \frac{4L_z nm((-1)^{n+m} - 1)}{\pi^2(m^2 - n^2)^2}, \quad (\text{A7})$$

$$R(n, m) = -2\sqrt{3} \frac{\hbar^2 \gamma_3}{2m_0} \frac{2inm((-1)^{n+m} - 1)}{L_z(n^2 - m^2)}. \quad (\text{A8})$$

Our aim is to perform a transformation which decouples the groups \mathcal{G}_1 from \mathcal{G}_2 , i.e. to make the off-diagonal part $\tilde{H}_{2 \times 6}$ and $\tilde{H}_{6 \times 2}$ vanish up to the first-order in k and F . We divide the total Hamiltonian (A1) into three parts

$$H_{8 \times 8} = H_0 + H_1 + H_2. \quad (\text{A9})$$

The first term H_0 is the diagonal matrix elements of $H_{8 \times 8}$, given by

$$H_0 = \begin{pmatrix} \tilde{H}_{2 \times 2}^{(0)} & 0 \\ 0 & \tilde{H}_{6 \times 6}^{(0)} \end{pmatrix}, \quad (\text{A10})$$

with $\tilde{H}_{2 \times 2}^{(0)} = \text{Diag}[P(1), P(1)]$ and $\tilde{H}_{6 \times 6}^{(0)} = \text{Diag}[Q(1), Q(1), P(2), P(2), Q(2), Q(2)]$.

The second term H_1 is given by

$$H_1 = \begin{pmatrix} 0 & 0 \\ 0 & \tilde{H}_{6 \times 6}^{(1)} \end{pmatrix}, \quad (\text{A11})$$

where $\tilde{H}_{6 \times 6}^{(1)} = \tilde{H}_{6 \times 6} - \tilde{H}_{6 \times 6}^{(0)}$. The third term H_2 contains the non-diagonal part $\tilde{H}_{2 \times 6}$ and $\tilde{H}_{6 \times 2}$

$$H_2 = \begin{pmatrix} 0 & \tilde{H}_{2 \times 6} \\ \tilde{H}_{6 \times 2} & 0 \end{pmatrix}. \quad (\text{A12})$$

There are three types of perturbation terms in H_1 and H_2 : (1) The k-linear R term couples the state $|n, \frac{3}{2}\rangle$ ($|n, -\frac{3}{2}\rangle$) with $|m, \frac{1}{2}\rangle$ ($|m, -\frac{1}{2}\rangle$), where n and m must be of opposite parities due to the presence of $k_z = -i\partial_z$; (2) The k-quadratic T term couples $|n, \frac{3}{2}\rangle$ ($|n, -\frac{3}{2}\rangle$) with $|n, -\frac{1}{2}\rangle$ ($|n, \frac{1}{2}\rangle$); (3) The asymmetric potential V_a couples the states with the same spin index and different parities.

The perturbation procedure is as follows. First H_2 will be eliminated by the canonical transformation as

$$\begin{aligned} H_{8 \times 8}^{(1)} &= \exp[-U^{(1)}] H_{8 \times 8} \exp[U^{(1)}] \\ &= H_{8 \times 8} + [H_{8 \times 8}, U^{(1)}] + \frac{1}{2} [[H_{8 \times 8}, U^{(1)}], U^{(1)}] \\ &\quad + \dots, \end{aligned} \quad (\text{A13})$$

in which $U^{(1)}$ is chosen such that

$$H_2 + [H_0, U^{(1)}] = 0,$$

and the matrix elements read

$$U_{\alpha\beta}^{(1)} = -\frac{(H_2)_{\alpha\beta}}{E_\alpha - E_\beta}, \quad \alpha \neq \beta, \quad (\text{A14})$$

where E_α denotes the energy of the band α at the Γ point ($k=0$). After the canonical transformation, the new Hamiltonian is given by

$$\begin{aligned} H_{8 \times 8}^{(1)} &= H_0 + H_1 + \frac{1}{2} [H_2, U^{(1)}] + [H_1, U^{(1)}] \\ &\quad + \frac{1}{2} [[H_1, U^{(1)}], U^{(1)}] + \dots \end{aligned} \quad (\text{A15})$$

The H_0 , H_1 , $\frac{1}{2}[H_2, U^{(1)}]$ and $\frac{1}{2}[[H_1, U^{(1)}], U^{(1)}]$ have the block-diagonal form, while $[H_1, U^{(1)}]$ is non-block-diagonal and contains new terms first-order in k . So we divide $H_{8 \times 8}^{(1)}$ into three parts again

$$H_{8 \times 8}^{(1)} = H_0 + H_1^{(1)} + H_2^{(1)}, \quad (\text{A16})$$

in which $H_1^{(1)} = H_1 + \frac{1}{2}[H_2, U^{(1)}] + \frac{1}{2}[[H_1, U^{(1)}], U^{(1)}]$, and $H_2^{(1)} = [H_1, U^{(1)}]$. We perform the second canonical transformation $U^{(2)}$, given by

$$U_{\alpha\beta}^{(2)} = -\frac{(H_2^{(1)})_{\alpha\beta}}{E_\alpha - E_\beta}, \quad \alpha \neq \beta. \quad (\text{A17})$$

This makes the non-diagonal block matrix $H_2^{(1)}$ zero, leading to the Hamiltonian

$$\begin{aligned} H_{8 \times 8}^{(2)} &= H_0 + H_1^{(1)} + \frac{1}{2} [H_2^{(1)}, U^{(1)}] + [H_1^{(1)}, U^{(1)}] \\ &\quad + \frac{1}{2} [[H_1^{(1)}, U^{(1)}], U^{(1)}] + \dots \end{aligned} \quad (\text{A18})$$

Now the non-block-diagonal terms of $H_{8 \times 8}^{(2)}$ vanish up to the desired order in k and F . Finally, by mapping the Hamiltonian $H_{8 \times 8}^{(2)}$ into the lowest heavy hole subbands, we obtain the k -cubic Rashba Hamiltonian Eq. (23).

To obtain the corresponding spin operators in the lowest heavy hole basis, we should apply the same canonical transformations $U^{(1)}$ and $U^{(2)}$ to the spin operators S_i ($i = x, y, z$). In the 8-state subspace \mathcal{G}_0 , we find that the spin operator has the block-diagonal form $S_i = \text{Diag}[S_i^{(1)}, S_i^{(1)}]$ ($i = x, y, z$), because there are no matrix elements between the states with different confinement quantum number n . Therefore $S_i^{(1)}$ is a 4×4 matrix, given respectively by

$$S_x^{(1)} = \frac{1}{2} \begin{pmatrix} 0 & 0 & \sqrt{3} & 0 \\ 0 & 0 & 0 & \sqrt{3} \\ \sqrt{3} & 0 & 0 & 2 \\ 0 & \sqrt{3} & 2 & 0 \end{pmatrix}, \quad (\text{A19})$$

$$S_y^{(1)} = \frac{i}{2} \begin{pmatrix} 0 & 0 & -\sqrt{3} & 0 \\ 0 & 0 & 0 & \sqrt{3} \\ \sqrt{3} & 0 & 0 & -2 \\ 0 & -\sqrt{3} & 2 & 0 \end{pmatrix}, \quad (\text{A20})$$

$$S_z^{(1)} = \frac{1}{2} \begin{pmatrix} 3 & 0 & 0 & 0 \\ 0 & -3 & 0 & 0 \\ 0 & 0 & 1 & 0 \\ 0 & 0 & 0 & -1 \end{pmatrix}. \quad (\text{A21})$$

Then we apply the transformations $U^{(1)}$ and $U^{(2)}$ to the spin operators, obtaining the new spin operators $\tilde{S}_i = S_i + [S_i, U^{(1)}] + [S_i, U^{(2)}]$ as presented in Eqs. (29), (30) and (31).

APPENDIX B: HOLE RASHBA TERM

The hole Rashba term has recently attracted many researchers' attentions.^{32,36,47} The hole Rashba term breaks the inversion symmetry,^{35,37} and is expressed as

$$\hat{H}_R = \lambda \begin{pmatrix} 0 & \frac{i\sqrt{3}}{2}k_- & 0 & 0 \\ -\frac{i\sqrt{3}}{2}k_+ & 0 & ik_- & 0 \\ 0 & -ik_+ & 0 & \frac{i\sqrt{3}}{2}k_- \\ 0 & 0 & -\frac{i\sqrt{3}}{2}k_+ & 0 \end{pmatrix}, \quad (\text{B1})$$

where $\lambda = r_{41}^{8v8v} F$, r_{41}^{8v8v} is a parameter as already given by Winkler for several materials,³⁵ and F is the field strength. If we neglect other asymmetrical potentials and only consider the Rashba term, then the total Hamiltonian is $\hat{H} = H_L + V_c + H_R$. Applying the same perturbation procedure as in the appendix A, we find that both the Hamiltonian and the spin operator have the identical structure to the asymmetrical potential case, as well as the same effective mass m_h , S_1 and expression Eq. (34), except for the Rashba coefficient given by

$$\alpha = \frac{3\lambda L_z^2}{4\pi^2}, \quad (\text{B2})$$

and the spin operator parameter

$$S_0 = \frac{3\lambda m_0 L_z^2}{4\pi^2 \hbar^2 \gamma_2}. \quad (\text{B3})$$

The hole Rashba coefficient α here is proportional to L_z^2 , while for the asymmetrical potential case it depends on L_z^4 . So in most realistic quantum wells, the contribution from the asymmetrical potential plays more important role than the hole Rashba term, at least one or two orders of magnitude larger. The physical reason for this may be understood from the origin of the hole Rashba term. The more general form of the Hamiltonian should be $\hat{H} = \hat{H}_{\mathbf{k}\cdot\mathbf{p}} + V_c + eFz$, where the multi-band $\mathbf{k} \cdot \mathbf{p}$ Hamiltonian $\hat{H}_{\mathbf{k}\cdot\mathbf{p}}$ includes not only the heavy and light hole bands, but also the conduction band, spin split-off band and remote bands. When we project the Hamiltonian into the subspace of the heavy and light hole bands, the combined effects of the eFz and $\mathbf{k} \cdot \mathbf{p}$ mediated by other bands lead to the hole Rashba term, which has much smaller influence than that coupled by the asymmetrical potential directly. Therefore, hole Rashba term is neglected in the present article for simplicity.

¹ I. Zutic, J. Fabian, and S. Das Sarma, Rev. Mod. Phys. **76**, 323 (2004).

² S. A. Wolf, D. D. Awschalom, R. A. Buhrman, J. M. Daughton, S. von Molna, M. L. Roukes, A. Y. Chtchelkanova, D. M. Treger, Science **294**, 1488 (2001).

³ D. D. Awschalom and M. E. Flatte, Nature Phys. **3**, 153 (2007).

⁴ M. I. Dyakonov and V. I. Perel, Phys. Lett. **35A**, 459 (1971).

⁵ V. M. Edelstein, Solid State Commun. **73**, 233 (1990).

⁶ A. G. Aronov, Yu. B. Lyanda-Geller, and G. E. Pikus, Sov. Phys. JETP **73**, 537 (1991).

⁷ A. V. Chaplik, M. V. Entin, and L. I. Magarill, Physica E (Amsterdam) **13**, 744 (2002).

⁸ J. I. Inoue, W. Bauer, and W. Molenkamp, Phys. Rev. B **67**, 033104 (2003).

⁹ O. Bleibaum, Phys. Rev. B **73**, 035322 (2006).

¹⁰ O. Bleibaum, Phys. Rev. B **72**, 075366 (2005).

- ¹¹ Y. J. Bao and S. Q. Shen, Phys. Rev. B **76**, 045313 (2007).
- ¹² A. Yu. Silov, P. A. Blajnov, J. H. Wolter, R. Hey, K. H. Ploog, and N. S. Averkiev, Appl. Phys. Lett **85**, 5929 (2004).
- ¹³ Y. Kato, R. C. Myers, A. C. Gossard and D. D. Awschalom, Nature (London) **427**, 50 (2004).
- ¹⁴ Y. Kato, R. C. Myers, A. C. Gossard, and D. D. Awschalom, Phys. Rev. Lett. **93** 176601 (2004).
- ¹⁵ V. Sih, R. C. Myers, Y. K. Kato, W. H. Lau, A. C. Gossard and D. D. Awschalom, Nature Physics, **1**, 31 (2005).
- ¹⁶ N. P. Stern, S. Ghosh, G. Xiang, M. Zhu, N. Samarth, and D. D. Awschalom, Phys. Rev. Lett. **97** 126603 (2006).
- ¹⁷ C. L. Yang, H. T. He, L. Ding, L. J. Cui, Y. P. Zeng, J. N. Wang, and W. K. Ge, Phys. Rev. Lett. **96**, 186605 (2006).
- ¹⁸ S. D. Ganichev, S. N. Danilov, P. Schneider, V. V. Belkov, L. E. Golub, W. Wegscheider, D. Weiss, W. Prettl, J. Magn. Mater. **300**, 127 (2006).
- ¹⁹ S. D. Ganichev and W. Prettl, J. Phys. Condens. Matter **15**, R935 (2003), and references therein.
- ²⁰ X. D. Cui, S. Q. Shen, J. Li, Y. Ji, W. K. Ge, and F. C. Zhang, Appl. Phys. Lett. **90**, 242115 (2007).
- ²¹ M. G. Vavilov, Phys. Rev. B **72**, 195327 (2005).
- ²² S. A. Tarasenko, Phys. Rev. B **72**, 153103 (2005).
- ²³ M. Trushin and J. Schliemann, Phys. Rev. B **75**, 155323 (2007).
- ²⁴ Z. A. Huang and L. B. Hu, Phys. Rev. B **73**, 113312 (2006).
- ²⁵ X. H. Ma, L. B. Hu, R. B. Tao, and S. Q. Shen Phys. Rev. B **70**, 195343 (2004).
- ²⁶ L. B. Hu, J. Gao, and S. Q. Shen, Phys. Rev. B **70**, 235323 (2004).
- ²⁷ B. Kaestner, D. G. Hasko, and D. A. Williams, cond-mat/0411130.
- ²⁸ B. Kaestner, PhD dissertation, University of Cambridge (2003).
- ²⁹ A. Yu. Silov, J. E. M. Haverkort, N. S. Averkiev, P. M. Koenraad, and J. H. Wolter, Phys. Rev. B **50**, 4509 (1994).
- ³⁰ J. M. Luttinger, and W. Kohn, Phys. Rev. **97**, 869 (1955); J. M. Luttinger, Phys. Rev. **102**, 1030 (1956).
- ³¹ B. A. Bernevig, T. L. Hughes and S. C. Zhang, Phys. Rev. Lett. **95**, 066601 (2005).
- ³² B. A. Bernevig and S. C. Zhang, Phys. Rev. Lett. **95**, 016801 (2005).
- ³³ J. Schliemann and D. Loss, Phys. Rev. B **71**, 085308 (2005).
- ³⁴ J. Sinova, S. Murakami, S. Q. Shen, and M. S. Choi, Solid State Communi. **138**, 214 (2006)
- ³⁵ R. Winkler, Spin-Orbit Coupling Effects in Two-Dimensional Electron and Hole Systems, (Springer-Verlag Berlin 2003).
- ³⁶ R. Winkler, Phys. Rev. B **62**, 4245 (2000).
- ³⁷ B. F. Zhu and Y. C. Chang, Phys. Rev. B **50**, 11932 (1994).
- ³⁸ G. D. Mahan, *Many-Particle Physics*, (Kluwer Academic, New York, 2000).
- ³⁹ P. Streda, J. Phys. C **15**, L717 (1982); L. Smrcka and P. Streda, J. Phys. C **10**, 2153 (1977).
- ⁴⁰ N. A. Sinitsyn, J. E. Hill, Hongki Min, Jairo Sinova, and A. H. MacDonald, Phys. Rev. Lett **97**, 106804 (2006).
- ⁴¹ S. Q. Shen and Z. D. Wang, Phys. Rev. B **61**, 9532 (2000)
- ⁴² B. A. Foreman, Phys. Rev. Lett, **84**, 2505 (2000).
- ⁴³ B. A. Foreman, Phys. Rev. B **72**, 165344 (2005).
- ⁴⁴ B. A. Foreman, Phys. Rev. B **72**, 165345 (2005).
- ⁴⁵ B. Habib, E. Tutuc, S. Melinte, M. Shayegan, D. Wasserman, S. A. Lyon, and R. Winkler, Phys. Rev. B **69**, 113311 (2004).
- ⁴⁶ K. Huang, J. B. Xia, B. F. Zhu, and H. Tang, J. Lumin. **40- 41**, 88 (1988)
- ⁴⁷ M. M. Hasegawa and E. A. de Andrada e Silva, Phys. Rev. B **68**, 205309 (2003).